



**HAL**  
open science

## HTRB Stress Effects on Static and Dynamic Characteristics of $0.15 \mu\text{m}$ AlGa<sub>N</sub>/Ga<sub>N</sub> HEMTs

P. Vigneshwara Raja, Jean-Christophe Nallatamby, Mohamed Bouslama, Jean-Claude Jacquet, Raphaël Sommet, Christophe Chang, Benoit Lambert

► **To cite this version:**

P. Vigneshwara Raja, Jean-Christophe Nallatamby, Mohamed Bouslama, Jean-Claude Jacquet, Raphaël Sommet, et al.. HTRB Stress Effects on Static and Dynamic Characteristics of  $0.15 \mu\text{m}$  AlGa<sub>N</sub>/Ga<sub>N</sub> HEMTs. IEEE Transactions on Microwave Theory and Techniques, 2023, 71 (5), pp.1957-1966. 10.1109/TMTT.2022.3222190 . hal-04176434

**HAL Id: hal-04176434**

**<https://hal.science/hal-04176434v1>**

Submitted on 14 Nov 2024

**HAL** is a multi-disciplinary open access archive for the deposit and dissemination of scientific research documents, whether they are published or not. The documents may come from teaching and research institutions in France or abroad, or from public or private research centers.

L'archive ouverte pluridisciplinaire **HAL**, est destinée au dépôt et à la diffusion de documents scientifiques de niveau recherche, publiés ou non, émanant des établissements d'enseignement et de recherche français ou étrangers, des laboratoires publics ou privés.

# HTRB Stress Effects on Static and Dynamic Characteristics of 0.15 $\mu\text{m}$ AlGaIn/GaN HEMTs

P. Vigneshwara Raja, Jean-Christophe Nallatamby, Mohamed Bouslama, Jean-Claude Jacquet, Raphael Sommet, Christophe Chang, and Benoit Lambert

**Abstract**—High temperature reverse bias (HTRB) stress effects on static and dynamic characteristics of 0.15  $\mu\text{m}$  AlGaIn/GaN high-electron mobility transistors (HEMTs) are reported. The HEMTs were stressed to off-state bias ( $V_{GS} = -7$  V,  $V_{DS} = 30$  V) at a high temperature of 175 °C for 1000 hours of duration. The HTRB induced changes in drain current ( $I_{DS}$ ) are analyzed. The  $I_G$ - $V_G$  characteristics are evaluated at  $V_{DS} = 0$  V (emulating gate Schottky diode leakage) before and after the stress to examine the Schottky gate diode properties upon aging. The gate leakage current variations are further inspected with  $V_G$  and  $V_D$  sweeps. After aging test, a considerable drift in the output power ( $P_{out}$ ) is observed during the interim RF measurement of the stressed HEMTs. The pulsed  $I_{DS}$ - $V_{DS}$  characteristics reveal the reduction in  $I_{DS}$ , particularly in the transition between linear and saturation regions; which is referred as knee-voltage smoothing. The output-admittance ( $Y_{22}$ ) and drain current transient (DCT) measurements are conducted to track any new defects created in the stressed HEMT and also assess the evolution of the preexisting trap parameters. Especially, physical location of the traps responsible for the knee-voltage smoothing and output power drift is identified by TCAD simulations.

**Index Terms**— AlGaIn/GaN HEMT, buffer trap, drain current, gate leakage, HTRB, power drift, reliability.

## I. INTRODUCTION

THE ultra-submicrometer AlGaIn/GaN HEMT devices have been proved to be effective for monolithic microwave integrated circuits (MMIC), RF power amplifiers (RFPAs), and high power switches. The GaN-based HEMT process technology has been optimized to deliver high output power and power-added efficiency (PAE)

*“This paper is an expanded version from the 2022 IEEE MTT-S International Conference on Numerical Electromagnetic and Multiphysics Modeling and Optimization, Limoges (France), July 6th-8th.”*

We greatly appreciate and acknowledge the Agence Nationale de la Recherche (ANR) and Direction Générale de l’Armement (DGA) project contributors, France for funding under contract ANR-17-ASTR-0007-01 (COMPACT project).

P. Vigneshwara Raja is with Department of Electrical Engineering, Indian Institute of Technology Dharwad, Karnataka-580011, India (e-mail: vigneshwararaja@iitdh.ac.in).

Jean-Christophe Nallatamby and Raphael Sommet are with the XLIM Laboratory, CNRS, UMR 7252, University of Limoges, F-19100 Brive, France (e-mail: jean-christophe.nallatamby@unilim.fr; raphael.sommet@xlim.fr).

Mohamed Bouslama and Jean-Claude Jacquet are with III-V Lab, 91120 Palaiseau, France (e-mail: mohamed.bouslama@3-5lab.fr; jean-claude.jacquet@3-5lab.fr).

Christophe Chang and Benoit Lambert are with United Monolithic Semiconductors, 10 avenue du Québec, 91140 Villebon-sur-Yvette, France (e-mail: christophe.chang@ums-rf.com; benoit.lambert@ums-rf.com).

up to 40 GHz, along with high linearity. Nevertheless, the long-term reliability of the HEMT still needs further improvement to extend the operational lifetime, in certain targeted applications like radar, satellite, and telecommunications. Before delivering the product to the market, the performance and reliability of the HEMT must be thoroughly checked to verify if the device will sustain the real-world environmental stresses and remain to meet future demands [1]-[3]. The accelerated bias aging test such as high temperature reverse bias (HTRB) encompasses elevated temperature storage and high gate-drain reverse bias to aggravate the various device failure modes with the Arrhenius acceleration factor; thus mean-time-to-failure (MTTF) of the device may be anticipated [1]-[3]. The reliability studies are useful to identify the root cause of the degradation mechanisms and some hidden failure modes, thereby allowing us to prevent those device failures. Moreover, some specific application areas of the HEMTs demand high power and temperature operation. These points signify the importance of the aging test. Therefore, this work is motivated to study the HTRB stress effects on the state-of-the-art 0.15  $\mu\text{m}$  AlGaIn/GaN HEMT characteristics.

The high gate leakage current of the AlGaIn/GaN HEMT is a crucial factor in affecting standby power dissipation, gate voltage swing, and device reliability [2]-[4]. So, a special emphasis is devoted to investigate the HTRB induced changes in the gate current. The gate leakage current variations are analyzed at  $V_{DS} = 0$  V bias state (imitating gate Schottky barrier diode) to inspect the metal/GaN/AlGaIn Schottky gate interface properties, compared to the pre-stress condition.

The electron trapping due to the deep-level defects in the HEMT restricts the maximum achievable drain current during the dynamic operation [5]-[7]. The electrically active traps may also promote the gate-leakage current conduction through trap-assisted tunneling and Poole-Frenkel emission mechanisms [3], [4]. Alamo *et al.* [2] reported that the off-state electrical stress produces electrically active traps in the AlGaIn barrier layer, near the gate edge region towards the drain side. The authors hypothesized that the stress produced defects are responsible for the drain current reduction and the gate current increase due to the defect-induced leakage paths. For this reason, low-frequency (LF) output-admittance ( $Y_{22}$ ) and drain current transient (DCT) spectroscopy characterizations are performed to track whether any new trap is created or not in the stressed HEMTs. In our earlier work [7]-[9], an acceptor-type electron trap at  $E_c - 0.5$  eV was

> REPLACE THIS LINE WITH YOUR MANUSCRIPT ID NUMBER (DOUBLE-CLICK HERE TO EDIT) <

identified in the 0.15  $\mu\text{m}$  AlGaIn/GaN HEMT with Fe-doped buffer; a similar HEMT structure is used in this study. Moreover, our earlier simulation results [6], [7], [9], [10] reveal the presence of the acceptor trap at  $E_c - 0.5$  eV in the GaN buffer layer. Hence, the  $Y_{22}$  and DCT measurements are also intended to quantify the emission time constant evolutions of the Fe-related acceptor trap at  $E_c - 0.5$  eV in the AlGaIn/GaN HEMT after the HTRB stress.

Recently, Magnier *et al.* [11] observed a significant drop in the output power ( $P_{out}$ ) during the interim RF measurement of the stressed AlGaIn/GaN HEMTs, along with the reduction in the drain current during the transition between the linear and saturation regions of the pulsed  $I_{DS}-V_{DS}$  characteristics (knee voltage smoothing). Several authors investigated the stress-induced changes in the drain current [2], [3], [11-22] and gate leakage current [2], [15]-[19], trap parameters [20]-[22], and RF power [11], [23], [24] of the GaN-based HEMTs. However, there is no solid evidence in the literature, reporting the physical location of the HTRB stress produced defects accountable for the output power drift. To extend the work of Magnier *et al.* [11], the spatial location of the traps responsible for the knee voltage smoothing effect and output power drift is identified through TCAD simulations. In addition to that, the HTRB stress effects on the drain and gate currents ( $I_{DS}$  and  $I_G$ ) of the AlGaIn/GaN HEMTs are analyzed. Therefore, these preliminary HTRB test results are expected to provide a fundamental understanding of the device failure mechanisms in the HEMT due to the aging in actual operating conditions.

The HEMT structure details, HTRB stress experiment, and HEMT characterization methods are given in Section II. The HTRB stress effects on the drain and gate current, and output power are discussed in Sections III-A to III-C. The post-stress  $Y_{22}$  and DCT results are described in Section II-D. The TCAD simulation results are presented in Section III-E.

## II. EXPERIMENT

The AlGaIn/GaN HEMT structure incorporates Fe-doped GaN buffer layer grown on silicon carbide substrate, followed by GaN channel layer, AlGaIn barrier layer, and GaN cap layer. The HEMT features an ultra-short gate length of 0.15 $\mu\text{m}$  with a gate width of 4 $\times$ 50  $\mu\text{m}$ , and silicon nitride passivation layer at the ungated surface.

### A. HTRB Stress Test

The HTRB stress tests were performed at IMS from the University of Bordeaux and then at UMS by Florent Magnier [11]. In HTRB experiment, the HEMTs were stressed to a profound off-state bias condition of  $V_{GS} = -7$  V and  $V_{DS} = 30$  V (i.e. effective reverse gate-drain voltage  $V_{GD} = -37$  V) at an elevated temperature of 175  $^\circ\text{C}$  for a longer time duration of 1000 hours. The Lakeshore cryogenic probe station TTPX was used for the HTRB experiments.

### B. HTRB Characterization

The drain current ( $I_{DS}$ ) and gate leakage current ( $I_G$ ) of the AlGaIn/GaN HEMTs were measured before and after the stress test by using the Agilent B1500A Semiconductor device

parameter analyzer. The RF output power ( $P_{out}$ ) of the HEMT was measured at a bias condition of  $V_{DS} = 20$  V and  $I_{DS} = 200$  mA/mm with an input signal frequency  $f = 9$  GHz, in various time intervals during the HTRB stress test [11]. This short interim characterization procedure was proposed to quantitatively evaluate the power drift phenomenon with time due to the aging test. The output power of the HEMT was recorded at 5 dB gain compression. The RF power measurements were conducted for different operating temperatures of 25  $^\circ\text{C}$ , 75  $^\circ\text{C}$ , and 125  $^\circ\text{C}$  to probe the thermal impacts on the output power drift.

Pulsed  $I_{DS}-V_{DS}$  measurements were carried out at three different quiescent points ( $V_{GSQ}, V_{DSQ}$ ) = (0 V, 0 V), (-7 V, 0V), and (-7 V, 30 V) to quantify the trapping effects in the dynamic performance of the stressed HEMTs, in relative to the unstressed devices. The pulse period and duty cycle for the pulsed  $I-V$  characterization were chosen 30  $\mu\text{s}$ , and 1  $\mu\text{s}$ .

The experimental setup for LF  $Y_{22}$  and DCT spectroscopy is given elsewhere [6]-[9]. After the aging test, the  $Y_{22}$  parameters were acquired at the same bias point of  $V_{DSQ} = 10$  V and  $I_{DSQ} = 50$  mA/mm in the low-frequency range of 100 Hz to 1 MHz for different temperatures from 25  $^\circ\text{C}$  to 125  $^\circ\text{C}$ . In DCT spectroscopy, a drain-lag pulsing scheme ( $V_{DS}$  switched from 10V to 20 V for 100 ms pulse width) was employed to populate the traps in the HEMT. Consequently,  $V_{DS}$  was reverted to its initial bias point ( $V_{DM} = 10$  V), and the emission transient was measured over 1  $\mu\text{s}$  to 1 s for temperatures ranging from 25  $^\circ\text{C}$  to 125  $^\circ\text{C}$ .

## III. RESULTS AND DISCUSSION

### A. Drain Current Characteristics

Figures 1(a) and 1(b) show the output ( $I_{DS}-V_{DS}$ ) and transfer ( $I_{DS}-V_{GS}$ ) characteristics (at  $T = 25$   $^\circ\text{C}$ ) of the AlGaIn/GaN HEMT before and after the HTRB stress. The drain current ( $I_{DS}$ ), and threshold voltage magnitude  $|V_{TH}|$  are reduced after the HTRB test. The on-resistance ( $R_{ON}$ ) of the HEMT increases after the stress, as identified from the linear region of the output drain current properties. Moreover, a positive shift in  $V_{TH}$  is noted from the transfer characteristics of the stressed HEMT, as seen in Fig. 1(b). These observations are consistent with the literature reports [11]-[22].

The reasons for  $I_{DS}$  reduction are discussed as follows: During the HTRB test, the HEMTs were subjected to thermally accelerated aging (with Arrhenius rate) and off-state electrical stress. The lattice phonon scattering effects are more pronounced at elevated temperatures [25]-[27], so channel electron mobility (low field mobility) is affected by the HTRB stress. Zhao *et al.* [28] observed a reduction in  $I_{DS}$  after the thermal storage of the HEMT due to the attenuation in the 2DEG density, caused by the interface relaxation and defect creation during the aging test. Wang *et al.* [25] found that the 2DEG density drops at higher temperatures due to the conduction band offset shrinking at the AlGaIn/GaN heterointerface. The  $I_{DS}$  reduction in the saturation region of the output characteristics is attributed to the alleviated high-field velocity, caused by the optical phonon scattering [26].

> REPLACE THIS LINE WITH YOUR MANUSCRIPT ID NUMBER (DOUBLE-CLICK HERE TO EDIT) <

Therefore, the possible reasons for the  $I_{DS}$  decline after the stress are decreased 2DEG density, low-field mobility, and high-field velocity. The static drain current characteristics reveal that the HTRB aging test deteriorates the current driving capability of the AlGaIn/GaN HEMTs.

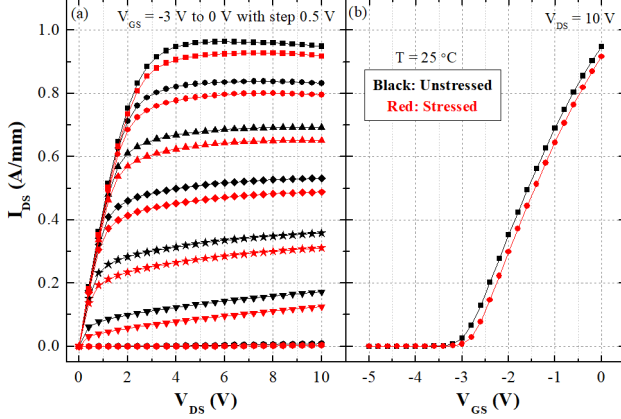


Fig. 1. (a) Output ( $I_{DS}$ - $V_{DS}$ ) and (b) transfer ( $I_{DS}$ - $V_{GS}$ ) characteristics of the AlGaIn/GaN HEMTs before and after the HTRB stress test.

### B. Gate Leakage Current

To analyze the gate Schottky contact properties, gate current ( $I_G$ ) is inspected at  $V_{DS} = 0$  V bias condition. The unstressed HEMT characteristics are discussed first. The forward  $I_G$ - $V_G$  properties for  $V_{DS} = 0$  V at 25 °C are shown in Fig. 2(a). Three different regions of current transport mechanisms are identified in the forward  $I_G$ - $V_G$ . As the diode saturation current may only govern the current transport in Region-1, nearly constant and low current ( $< 10$  pA) is observed. Beyond that, two linear regions (R2 and R3) with different slopes are noticed in the forward  $I_G$ - $V_G$ . In general, the series resistance effect comes into the picture at higher current levels (at higher forward voltages) of the Schottky barrier diode characteristics [29], [30]. However, the series resistance combination may not produce a linear region in the semilog forward I-V plot. The region-3 characteristics are fitted by using the standard thermionic emission (TE) model [29], [30], specifying that two different Schottky barrier heights exist at metal/GaN Schottky interface [31], [32]. So, it is considered that the gate Schottky contact consists of two diodes positioned in a back-to-back series arrangement [31]. The Schottky barrier height (SBH) and ideality factor ( $n$ ) for the two linear regions are calculated as per the standard TE model expressions [29], [30], [32]

$$SBH = (kT/q) \ln(A^*T^2/J_s) \quad (1)$$

$$n = (q/kT)[dV_F/d(\ln J_F)] \quad (2)$$

where  $A^*$  is the effective Richardson's constant for GaN ( $A^* = 26.9$  A cm<sup>-2</sup> K<sup>-2</sup> [33]),  $J_s$  is the reverse saturation current density,  $T$  is the temperature,  $k$  is the Boltzmann's constant,  $q$  is the electric charge,  $V_F$  and  $J_F$  represent the forward gate voltage and current density, respectively. The SBH at 25 °C for the diode-1 and 2 is extracted as 1.15 eV (SBH-1) and 0.72eV (SBH-2) using Eqns. 1 and 2. The ideality factor ( $n$ )

for the two diodes is found to be 1.66 (n1) and 4.36 (n2) at 25 °C. The two-diode model of Greco *et al.* [31] suggests that the first diode is associated with the typical metal/GaN cap interface. While the second diode may be related to the AlGaIn/GaN interface. In this case, SBH-2 indicates the energy difference between the Fermi level of AlGaIn/GaN interface and the GaN conduction band [31].

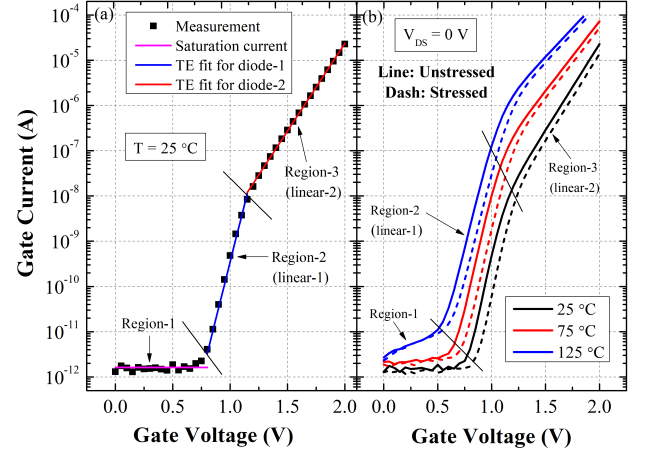


Fig. 2. (a) The forward  $I_G$ - $V_G$  properties at  $V_{DS} = 0$  V ( $T = 25$  °C) show three different regions of operation. (b) The forward  $I_G$ - $V_G$  of the unstressed and stressed HEMTs at 25 °C, 75 °C, and 125 °C.

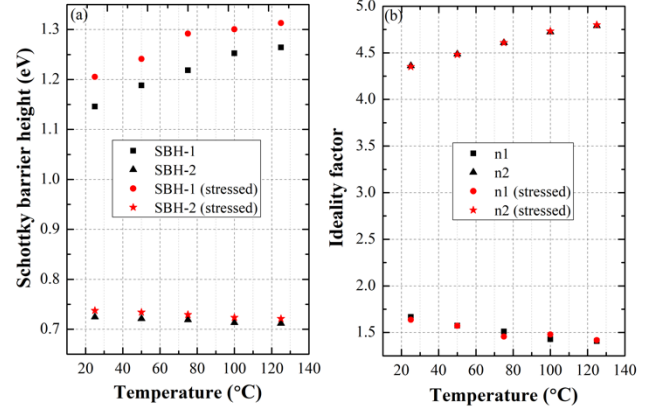


Fig. 3. Temperature dependence (25 °C to 125 °C) of Schottky barrier height (SBH) and ideality factor ( $n$ ) extracted from thermionic emission theory for two-diode model, before and after the stress.

The temperature dependence of SBH and  $n$  for the two-diode model is extracted [29], [30], [32] from forward I-V characteristics at different temperatures (25 °C to 125 °C) and are plotted in Figs. 3 (a) and (b). It is perceived that the SBH-1 (1.15 eV to 1.26 eV) increases and  $n1$  (1.66 to 1.4) decreases with the increasing temperature (opposite to the expected variation [33]); this behavior can be attributed to the inhomogeneous Schottky barrier existing [29]-[33] at metal/semiconductor interface on the GaN/AlGaIn/GaN heterostructure. The second-diode parameters such as SBH-2 (0.72-0.71 eV) and  $n2$  (4.36-4.79) have shown a weak temperature dependency from 25 °C to 125 °C. But the ideality factor ( $\sim 4.4$ ) of the second diode largely deviates from the ideal value ( $n = 1$ ) even at room temperature.

> REPLACE THIS LINE WITH YOUR MANUSCRIPT ID NUMBER (DOUBLE-CLICK HERE TO EDIT) <

Figure 2(b) shows forward  $I_G$ - $V_G$  of the unstressed and stressed HEMTs at different temperatures (25 °C to 125 °C). A small reduction in the forward  $I_G$  is noticed after the HTRB test. From Fig. 3(a), it is noted that the SBH-1 increases after the stress. Whereas, there is no considerable change in the SBH-2 for the second diode. The electron mobility is reduced during the HTRB stress test owing to the lattice phonon scattering, defect-induced scattering, and conduction band offset shrinking. Accordingly, the slight decrease in the forward  $I_G$  is attributed to the mobility degradation and the corresponding increase in the SBH-1 upon the stress test, since the standard TE theory controls the forward current transport of the gate Schottky barrier diode.

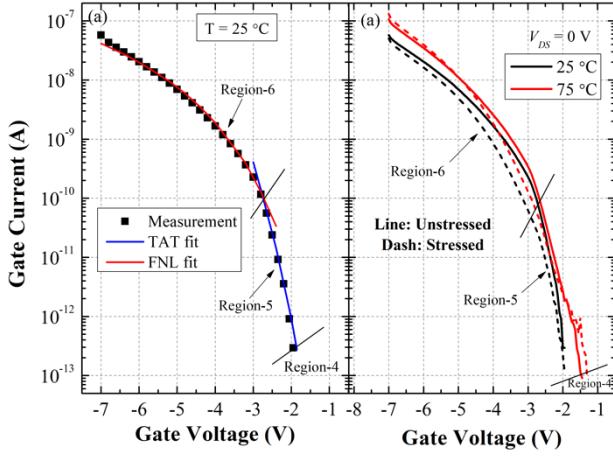


Fig. 4. (a) The reverse  $I_G$ - $V_G$  at  $V_{DS} = 0$  V ( $T = 25$  °C) indicate three different regions of operation. (b) The reverse  $I_G$ - $V_G$  of the unstressed and stressed HEMTs at 25 °C and 75 °C.

The reverse  $I_G$ - $V_G$  properties (at  $V_{DS} = 0$  V) in Fig. 4(a) demonstrate three different regions of operation. Since the reverse saturation current conduction may only occur for the bias voltage  $> -2$  V, the leakage current is found to be too low ( $< 10^{-13}$  A) in Region-4; the negative values are ignored in the semilog reverse  $I_G$ - $V_G$  plot. The electric field versus the gate voltage has to be estimated to identify the reverse gate current transport mechanisms. So, the electric field profile is computed from the TCAD simulation of AlGaIn/GaN HEMT and is used for the curve fitting analysis of the measured gate current. Figure 4(a) illustrates that trap-assisted tunneling (TAT) [34] is responsible for the current conduction in Region-5. The TAT leakage current ( $I_{TAT}$ ) generation due to the electron tunneling from the gate metal to the GaN channel through the band localized traps in the AlGaIn barrier can be symbolized as follows [34], [35]:

$$I_{TAT} = A \times C_{TAT} \times \exp\left(-\frac{8\pi\sqrt{2qm^*}}{3hE} \phi_r^{3/2}\right) \quad (3)$$

where  $A$  is the diode active area,  $C_{TAT}$  is the constant,  $m^*$  is the electron effective mass,  $h$  is the Planck's constant,  $E$  is the electric field,  $\phi_r$  is the energy level of the trap positioned below the conduction band at  $E_C - E_T$ . In Region-6, the reverse gate current is entirely governed by the Fowler-Nordheim tunneling (FNT) [4], [36] process, as identified from the curve

fitting of the experimental data (refer to Fig. 4). Triangular barrier formation occurs at higher reverse gate voltages, resulting in a penetration of electrons along the gate metal Fermi level from the gate edge to the GaN channel (through the AlGaIn barrier). The resultant FNT current ( $I_{FNT}$ ) can be modeled by [4], [29], [36]

$$I_{FNT} = A \times C_{FNT} \times E^2 \exp(-B/E) \quad (4)$$

$$B = \frac{8\pi\sqrt{2m^*}(q\Phi_{eff})^3}{3qh} \quad (5)$$

where  $C_{FNT}$  is constant, and  $\Phi_{eff}$  is the effective barrier height.

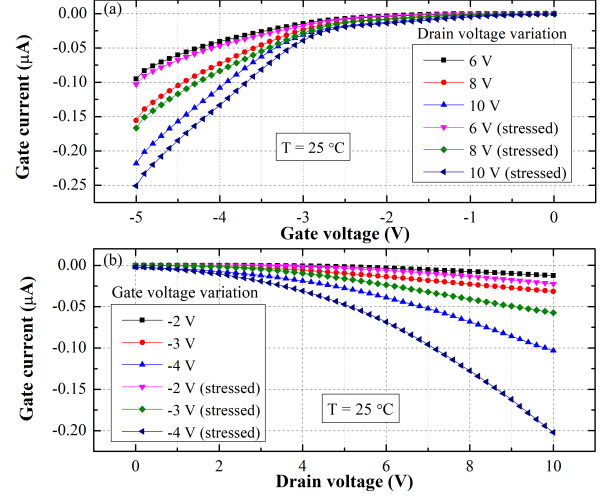


Fig. 5. (a)  $I_G$ - $V_G$  for various drain voltages of 6 V, 8 V and 10 V and (b) Gate current vs. drain voltage for different  $V_G$  (-2 V, -3 V, -4 V) for unstressed and stressed HEMTs at 25 °C.

In many reports [4], [36], [37], the electric field variation was considered to be constant beyond the threshold voltage ( $< -V_{TH}$ ) because of the depletion of 2DEG under the gate. On the contrary, it is noticed from Fig. 4 that the leakage current increases rapidly beyond  $V_{TH}$  due to the increase in the surface potential, as similar to the observations of Ghosh *et al.* [38]. Figure 4(b) shows the reverse  $I_G$ - $V_G$  of the unstressed and stressed HEMT for two temperatures 25 °C and 75 °C; only a minor change in the gate leakage current is noted after the aging test. It is reported [39], [40] that the Ohmic (Ti/Al/Ni/Au) and Schottky (Ni/Au) contacts of the AlGaIn/GaN HEMT system have a good thermal stability up to an elevated temperature of 300 °C. These points suggest that the gate Schottky contact properties were not affected by the HTRB stress test.

Figure 5(a) depicts the HTRB stress-induced changes in  $I_G$ - $V_G$  characteristics for various drain voltages ( $V_{DS} = 6$  V to 10 V) at 25 °C. It is clear that gate current increases with respect to  $V_G$  for different  $V_{DS}$  upon the aging test, supporting the literature reports [17]-[19]. The  $I_G$  increase is more pronounced at higher  $V_{DS}$  values. The gate current versus drain voltage properties for different  $V_G$  (-2 V to -4 V) are considerably increased in the stressed HEMTs, as illustrated in Fig. 5(b). The increase in the gate leakage current with the  $V_G$  and  $V_D$  sweep suggests that the HTRB stress may induce



> REPLACE THIS LINE WITH YOUR MANUSCRIPT ID NUMBER (DOUBLE-CLICK HERE TO EDIT) <

leakage current paths through the creation of electrically active defects in the barrier layer, referring to the work of Alamo *et al.* [2], [13]. From gate current characteristics, it is concluded that there is no significant change in the gate Schottky barrier diode properties after the aging test. At the same time, the gate leakage current increases with augmentation in the gate and drain voltages due to the HTRB stress produced defects in the AlGaIn barrier layer.

### C. Output Power Drift

Figure 6 shows the changes in the output power (at 5 dB gain compression and for signal frequency  $f = 9$  GHz) of two HEMTs (named A and B) measured in various time intervals during the HTRB stress testing. The output power is considerably decreased (i.e. power drift) after the first interim measurement at 5 minutes. The output power continues to decline with the subsequent interim measurement time (15, 30, and 60 minutes) during the stress experiment. The output power variation with the time is plotted at different temperatures (25 °C, 75 °C, and 125 °C) in Fig. 6. It is seen that the power drift phenomenon is more pronounced when the temperature is increased from 25 °C to 125 °C. Hence, the temperature is an acceleration factor for aggravating power drift behavior in the stressed HEMTs, analogous to the readings of Magnier *et al.* [11]. Overall, the RF output power is significantly reduced about 0.6 dB upon the first hour of the HTRB stress test, thereby degrading the RF and microwave performance of the AlGaIn/GaN HEMTs.

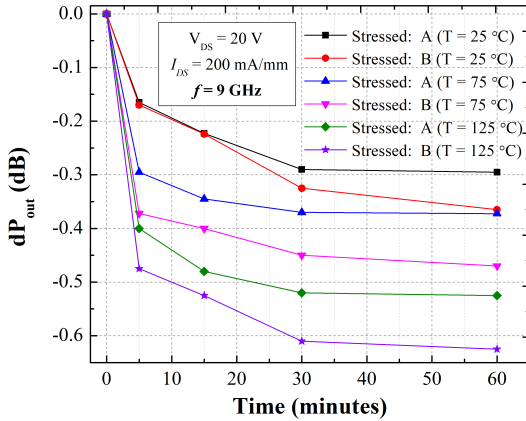


Fig. 6. Output power (at 5 dB gain compression and for signal frequency  $f = 9$  GHz) of the two HEMTs (A and B) measured in various time intervals (5, 15, 30 and 60 minutes) during the HTRB aging test and for different temperatures 25 °C, 75 °C, and 125 °C.

The pulsed  $I_{DS}$ - $V_{DS}$  characteristics of the stressed HEMTs are analyzed to correlate the trapping-induced dynamic reduction in drain current with the output power drift [11]. Figure 7 depicts pulsed  $I_{DS}$ - $V_{DS}$  characteristics (at  $V_{GS} = 0$  V) of unstressed and stressed AlGaIn/GaN HEMTs measured at different quiescent points ( $V_{GSQ}$ ,  $V_{DSQ}$ ) = (0 V, 0 V), (-7 V, 0 V), and (-7 V, 30 V). Negligible electron trapping in the HEMT is anticipated at the initial quiescent point ( $V_{GS}$ ,  $V_{DSQ}$ ) = (0 V, 0 V) [41]; as a result, no notable change in the drain

current is noticed in Fig. 7. Exposure to the negative gate quiescent bias condition ( $V_{GS}$ ,  $V_{DSQ}$ ) = (-7 V, 0 V) may promote electron trapping mechanism in the HEMT [8], [42]. For this reason,  $I_{DS}$  is decreased from its reference value, as perceived in the pulsed output characteristics. On the other hand, the deeper off-state quiescent reverse bias ( $V_{GDQ} = -37$  V) can induce strong trapping phenomena in the buffer and barrier layers of the AlGaIn/GaN HEMT [41]; so that a drastic reduction in  $I_{DS}$  is noticed in the case of ( $V_{GSQ}$ ,  $V_{DSQ}$ ) = (-7 V, 30 V), i.e. displaying typical trapping behavior in the HEMTs. Nonetheless, for all these cases, the drain current reduction is found to be larger in the stressed HEMTs, than in the unstressed devices. Particularly  $I_{DS}$  is substantially reduced during the evolution between the linear and saturation regions of the pulsed output properties for ( $V_{GSQ}$ ,  $V_{DSQ}$ ) = (-7 V, 30 V). Moreover, the transition between the linear and saturation regime becomes smoother; this effect is referred to as knee-voltage smoothing. The knee-voltage and current ( $V_{knee}$  and  $I_{knee}$ ) are interlinked with the RF output power ( $P_{out}$ ), as per the following expression [11]

$$P_{out} = \frac{I_{knee}}{2\pi} \frac{2\varphi - 2\sin(2\varphi)}{1 - \cos(\varphi)} \frac{V_{CL} - V_{knee}}{4} \quad (6)$$

where  $\varphi$  denotes the conduction angle, viz. ratio between maximum  $I_{DS}$  extracted from pulsed  $I$ - $V$  curve, and the drain bias current considered for the load-pull characterization.  $V_{CL}$  indicates the peak voltage during the load cycle [11]. Eqn. 3 denotes that the observed reduction in the knee voltage and current (knee-voltage smoothing) and the output power drift are the consequences of the HTRB stress-induced effects in the HEMT. The literature reports [2], [11], [16] suggest that the stress-produced defects in the AlGaIn/GaN HEMT are primarily responsible for the output power drift and knee-voltage smoothing effects. To check whether any new trap is created or not in the stressed HEMTs, LF  $Y_{22}$  and DCT characteristics are analyzed and are presented below.

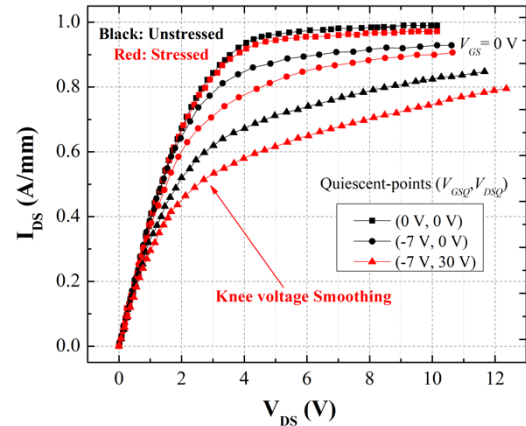


Fig. 7. Pulsed  $I_{DS}$ - $V_{DS}$  characteristics (at  $V_{GS} = 0$  V) of unstressed and stressed AlGaIn/GaN HEMTs measured at different quiescent points ( $V_{GSQ}$ ,  $V_{DSQ}$ ) = (0 V, 0 V), (-7 V, 0 V), and (-7 V, 30 V).

#### D. LF $Y_{22}$ and DCT Spectroscopy

Figure 8 shows the LF  $Y_{22}$  parameters of the Fe-doped AlGaIn/GaN HEMT measured before and after the aging test for different temperatures (25 °C to 125 °C). Arrhenius plots for the Fe-related trap [7]-[10], [42] identified from the  $Y_{22}$  and DCT spectroscopy for unstressed and stressed HEMTs are plotted in Fig. 9. Prior to the HTRB stress test, Arrhenius analysis [5]-[10] of the  $Y_{22}$  frequency dispersion properties yields the trap activation energy of  $E_c - 0.47$  eV and capture cross-section ( $\sigma_n$ ) of  $1.2 \times 10^{-15}$  cm<sup>2</sup>, based on the following equation [6], [7]

$$\ln(\tau_n T^2) = E_a / kT - \ln(\sigma_n v_{th} N_C / T^2) \quad (7)$$

where  $E_a$  is activation energy,  $\tau_n$  is the emission time constant,  $T$  is the temperature,  $N_C$  is the effective density of states in the conduction band,  $v_{th}$  is the carrier thermal velocity, and  $k$  is the Boltzmann's constant. Figure 8 shows that the emission rate of the trap is reduced at each temperature upon the stress. Accordingly, a small increase in the trap energy ( $E_c - 0.49$  eV) is obtained with an identical  $\sigma_n = 1.7 \times 10^{-15}$  cm<sup>2</sup> from the post-stress  $Y_{22}$  experiments. This suggests that the potential barrier for the electron emission from the trap level is bit increased upon aging; thus a little higher thermal activation energy is computed for the Fe-related acceptor trap in the buffer. The decrease in the  $Y_{22}$  signal magnitude after the aging test is due to the corresponding reduction in the drain current (see Fig. 1). However, no new traps are detected in the stressed HEMTs by the  $Y_{22}$  parameters.

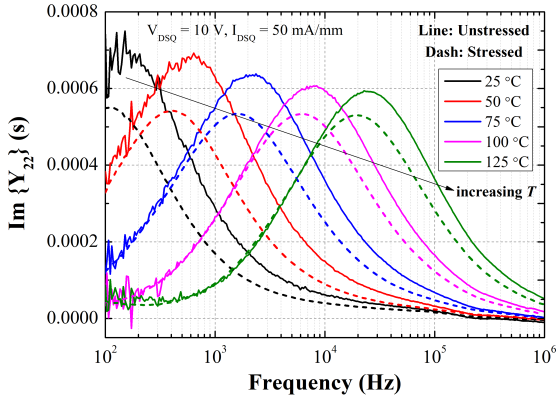


Fig. 8. LF  $Y_{22}$  parameters of the HEMT measured before and after the HTRB stress test at different temperatures (25 °C to 125 °C).

Figure 10(a) shows the DCT spectroscopy of the unstressed and stressed Fe-doped AlGaIn/GaN HEMTs in the temperature range of 25 °C to 125 °C and their DCT derivative spectra are plotted in Fig. 10(b). From DCT spectroscopy, a small increase in the emission time constant is noted after the stress experiments. However, almost the same trap parameters are attained for the unstressed ( $E_c - 0.5$  eV,  $3.5 \times 10^{-16}$  cm<sup>2</sup>) and the stressed ( $E_c - 0.51$  eV,  $4.5 \times 10^{-16}$  cm<sup>2</sup>) HEMTs, from the Arrhenius plot analysis. One point is evident from  $Y_{22}$  and DCT that the emission time constant of the trap slightly increases after the HTRB stress test, but that is not sufficient enough to change the trap activation energy noticeably.

Our earlier findings [5]-[10], [42] indicate that the  $Y_{22}$  and DCT techniques are effective in identifying traps in the GaN buffer layer. In this work, no new trap is determined after the aging test. Hence, the traps responsible for the knee-voltage smoothing behavior in the stressed HEMT are not identified by means of  $Y_{22}$  and DCT characterizations. Alamo [2], [16] and Magnier *et al.* [11] hypothesized that the off-state electrical stress can produce electronic trap levels in the AlGaIn barrier layer through inverse piezoelectric effect, and those defects are more detrimental in undermining the HEMT performance. Bearing these points in mind, TCAD simulations are performed by including acceptor traps in the barrier layer. The resultant changes in the  $I$ - $V$  characteristics for the AlGaIn/GaN HEMT are investigated and presented below.

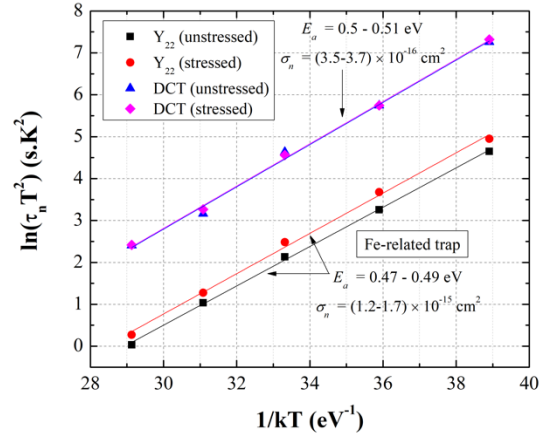


Fig. 9. Arrhenius plots for the Fe-related trap identified from the  $Y_{22}$  and DCT spectroscopy for unstressed and stressed HEMTs.

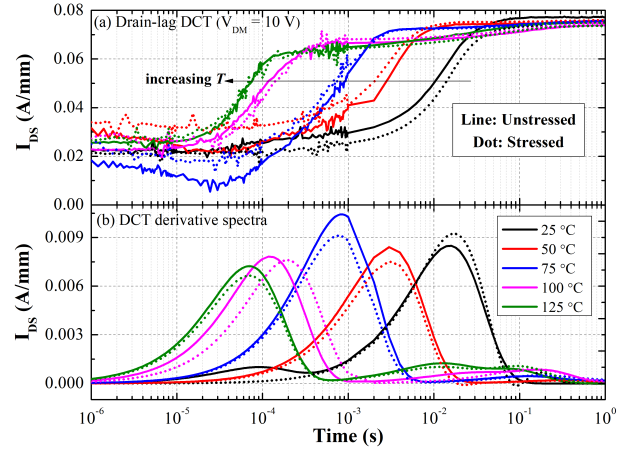


Fig. 10. (a) DCT spectroscopy of the unstressed and stressed Fe-doped AlGaIn/GaN HEMTs in the temperature range of 25 °C to 125 °C and (b) the corresponding DCT derivative spectra.

#### E. TCAD Simulation Results

It should be noted that the knee-voltage smoothing ( $I_{DS}$  reduction in between linear and saturation zones) is the prime reason for the power drift phenomenon [11]. So, the objective of the simulation is to identify the physical location of the traps responsible for the knee-voltage smoothing arising upon the HTRB test. The typical 2D cross-section of the 0.15  $\mu$ m

> REPLACE THIS LINE WITH YOUR MANUSCRIPT ID NUMBER (DOUBLE-CLICK HERE TO EDIT) <

AlGaIn/GaN HEMT structure is taken for the Sentaurus TCAD simulation. The physical models used in the simulation are discussed elsewhere [6], [7], [9], [10]. Three different electron trap energies such as  $E_c - 0.53$  eV,  $E_c - 0.73$  eV, and  $E_c - 0.93$  eV with a trap concentration of  $10^{18}$  cm<sup>-3</sup> are selected from the literature data [5], [7], [43]-[46]. During the stress test, the power drift is induced by the reduction in the drain current due to the electron capturing process associated with the traps. For this reason, acceptor-like traps are considered in the AlGaIn barrier. As represented in Fig. 11, the acceptor traps (one trap at a time  $E_c - 0.53$  eV /  $E_c - 0.73$  eV /  $E_c - 0.93$  eV) are placed at four different locations of the AlGaIn barrier layer in a rectangular spatial arrangement (size 25 nm  $\times$  22 nm): (i) drain side of the gate, (ii) drain side of the gate-edge, (iii) source side of the gate, and (iv) source side of the gate-edge. The traps have a discrete energy level, with a uniform concentration, placed at four different locations, but taken one position at a time. Subsequently, the changes in the output and transfer drain current characteristics of the HEMTs are analyzed.

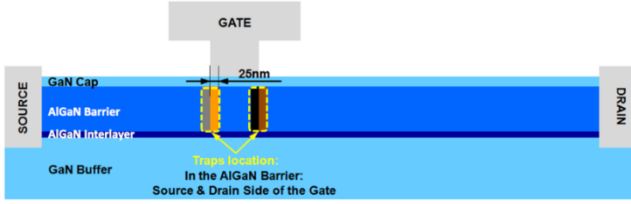


Fig. 11. Acceptor traps ( $E_c - 0.53$  eV /  $E_c - 0.73$  eV /  $E_c - 0.93$  eV) are placed (one trap at a time) at four different locations of the AlGaIn barrier layer with a rectangular fashion (size 25 nm  $\times$  22 nm): (i) drain side of the gate, (ii) drain side of the gate-edge, (iii) source side of the gate, and (iv) source side of the gate-edge.

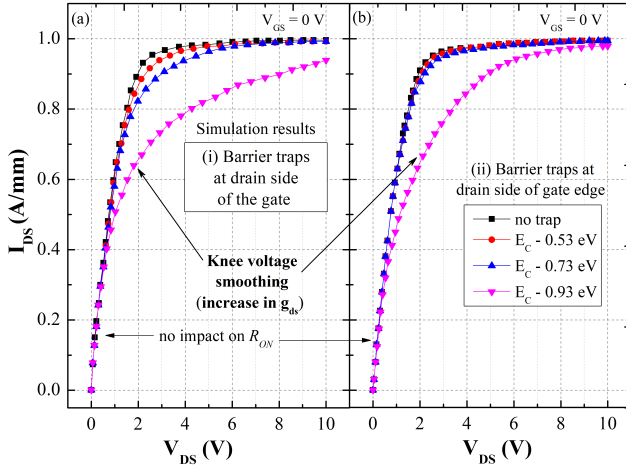


Fig. 12. Simulated output ( $I_{DS}$ - $V_{DS}$ ) characteristics of the AlGaIn/GaN HEMT at different barrier trap energies show the knee-voltage smoothing behavior for the spatial locations (a) drain side of the gate and (b) drain side of the gate edge.

Figures 12(a) and (b) show the simulated output ( $I_{DS}$ - $V_{DS}$ ) characteristics of the AlGaIn/GaN HEMT at different barrier trap energies for the spatial locations (i) drain side of the gate and (ii) drain side of the gate edge. The knee-voltage smoothing is observed in the simulated output characteristics after including the acceptor trap in the barrier layer at the drain

side of the gate and the gate edge, especially for deeper trap energies ( $> 0.73$  eV). Due to the knee-voltage smoothing effect, the output conductance ( $g_{ds}$ ) of the HEMT is reduced, which can decrease the RF output power. The on-resistance ( $R_{ON}$ ) of the HEMT is almost unaffected for these two cases, as seen in Figs. 12(a) and (b). There is no notable change in the threshold voltage of the HEMT, as observed (in Fig. 13) from the simulated transfer ( $I_{DS}$ - $V_{GS}$ ) properties at different barrier trap energies for the first two cases. Whereas the knee-voltage smoothing is not observed by placing the trap in the following locations: (iii) source side of the gate, and (iv) source side of the gate edge. The same behavior is displayed in Figs. 14(a) and (b), simulated output characteristics for the other two cases. Therefore, the simulation results indicate that the defects located in the AlGaIn barrier layer at the drain side of the gate and the gate edge regions, smooth the drain current transition between linear and saturation regions of the output characteristics.

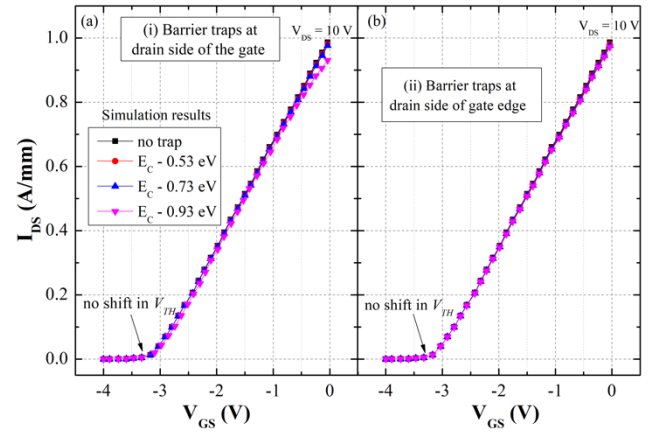


Fig. 13. Simulated transfer ( $I_{DS}$ - $V_{GS}$ ) properties of the AlGaIn/GaN HEMT at different barrier trap energies for the cases (a) drain side of the gate and (b) drain side of the gate edge.

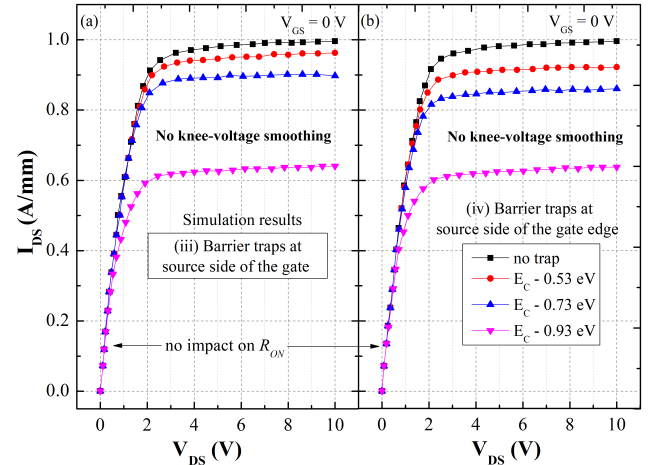


Fig. 14. Simulated output characteristics of the AlGaIn/GaN HEMT at different barrier trap energies for the cases (a) source side of the gate and (b) source side of the gate edge.

According to the simulation results, the observed power drift after the stress is attributed to the defect creation in the AlGaIn barrier at the drain side of the gate and the gate edge



regions, which can be explained as follows: During the HTRB test, a peak electric field occurs near the drain side of the gate vicinity due to the high gate-drain reverse voltage ( $V_{GD} = -37$  V) [47]. The strong off-state electric field and high-temperature induced Arrhenius acceleration effect may generate traps in the AlGaN barrier layer, specifically near the gate edge region towards the drain side [2], [16]. At this sub-threshold operation, the gate tunneling current injects electrons into the AlGaN barrier layer, and they get trapped by the stress-produced acceptor traps in the barrier layer. The barrier traps near the drain side of the gate edge may capture electrons from the 2DEG located around the source-drain access region. Thus, when the HEMT instantaneously switches from off-state to on-state during the RF operation, the drain current reduces due to the electron trapping in the barrier traps. This dynamic reduction in the drain current is visualized as knee-voltage smoothing in the pulsed output characteristics. Eventually, the RF output power of the HEMT is decreased by  $\sim 0.6$  dB during the first hour of the HTRB aging experiment.

#### IV. CONCLUSION

The HTRB stress effects on the AlGaN/GaN HEMTs are reported. The static drain current is reduced upon the aging test due to the reduction in 2DEG density, low-field mobility and high-field velocity. The forward  $I_G$ - $V_G$  at  $V_{DS} = 0$  shows that the gate interface comprises two different Schottky barrier heights. There is no significant change in reverse  $I_G$ - $V_G$  at  $V_{DS} = 0$  after the HTRB test, indicating that the gate Schottky contact properties are retained. No new trap is created in the GaN buffer layer after the stress test, as found from post-stress  $Y_{22}$  and DCT measurements. Moreover, only a small reduction in the emission rate of the Fe-related trap at  $E_c - 0.5$  eV is detected; still, typically the same trap parameters are obtained. The simulation results reveal that the off-state electrical and thermal stresses may create electrically active defects in the AlGaN barrier at the drain side of the gate and the gate edge regions, thereby smoothing the  $I_{DS}$  transition in between the linear and saturation region of the pulsed  $I_{DS}$ - $V_{DS}$  characteristics. As a result, the output power drifts up to 0.6dB during the interim RF measurement of the stressed AlGaN/GaN HEMTs. These preliminary HTRB test results are useful to understand the fundamental failure mechanisms of the HEMT due to the aging in actual operating conditions.

#### ACKNOWLEDGMENT

The authors would like to thank Dr. F. Magnier for useful discussions and HTRB stress tests.

#### REFERENCES

- [1] R. J. Trew, D. S. Green, and J. B. Shealy, "AlGaN/GaN HFET reliability," *IEEE Microw. Mag.*, vol. 10, no. 4, pp. 116-127, Jun. 2009.
- [2] J. A. D. Alamo and J. Joh, "GaN HEMT reliability," *Microelectron. Reliab.*, vol. 49, nos. 9-11, pp. 1200-1206, Nov. 2006.
- [3] G. Meneghesso, M. Meneghini, A. Tazzoli, A. Stocco, A. Chini, and E. Zanoni, "Reliability issues of gallium nitride high electron mobility transistors," *Int. J. Microw. Wirel. Technol.*, vol. 2, no. 1, pp. 39-50, Mar. 2010.
- [4] A. Debnath, N. DasGupta, and A. DasGupta, "Charge-based compact model of gate leakage current for AlInN/GaN and AlGaN/GaN HEMTs," *IEEE Trans. Electron Devices.*, vol. 67, no. 3, pp. 834-840, Mar. 2020.
- [5] J. Bergsten, M. Thorsell, D. Adolph, J.-T. Chen, O. Kordina, E. Ö. Sveinbjörnsson, and N. Rorsman, "Electron trapping in extended defects in microwave AlGaN/GaN HEMTs with carbon-doped buffers," *IEEE Trans. Electron Devices*, vol. 65, no. 6, pp. 2446-2453, Jun. 2018.
- [6] P. V. Raja, M. Bouslama, S. Sarkar, K. R. Pandurang, J.-C. Nallatamby, N. DasGupta, and A. DasGupta, "Deep-level traps in AlGaN/GaN and AlInN/GaN based HEMTs with different buffer doping technologies," *IEEE Trans. Electron Devices*, vol. 67, no. 6, pp. 2304-2310, Jun. 2020.
- [7] M. Bouslama, P. V. Raja, F. Gaillard, R. Sommet, and J.-C. Nallatamby, "Investigation of electron trapping in AlGaN/GaN HEMT with Fe-doped buffer through DCT characterization and TCAD device simulations," *AIP Adv.*, vol. 11, Dec. 2021, Art. no. 125316.
- [8] M. Bouslama, V. Gillet, C. Chang, J.-C. Nallatamby, R. Sommet, M. Prigent, R. Quéré, and B. Lambert, "Dynamic performance and characterization of traps using different measurements techniques for the new AlGaN/GaN HEMT of 0.15- $\mu$ m ultrashort gate length," *IEEE Trans. Microw. Theory Techn.*, vol. 67, no. 7, pp. 2475-2482, Jul. 2019.
- [9] P. V. Raja, N. K. Subramani, F. Gaillard, M. Bouslama, R. Sommet, and J.-C. Nallatamby, "Identification of buffer and surface traps in Fe-doped AlGaN/GaN HEMTs using Y21 frequency dispersion properties," *Electronics*, vol. 10, no. 24, Dec. 2021, Art. no. 3096.
- [10] P. V. Raja, J.-C. Nallatamby, N. DasGupta, and A. DasGupta, "Trapping effects on AlGaN/GaN HEMT characteristics," *Solid-State Electron.*, vol. 176, Feb. 2021, Art. no. 107929.
- [11] F. Magnier, B. Lambert, C. Chang, A. Curutchet, N. Labat, and N. Malbert, "Investigation of trap induced power drift on 0.15  $\mu$ m GaN technology after aging tests," *Microelectron. Reliab.*, vol. 100-101, Sep. 2019, Art no. 113358.
- [12] Z. Gao, M. Meneghini, F. Rampazzo, M. Rzin, C. D. Santi, G. Meneghesso, and E. Zanoni, "Reliability comparison of AlGaN/GaN HEMTs with different carbon doping concentration," *Microelectron. Reliab.*, vol. 100, Sep. 2019, Art. no. 113489.
- [13] T.-G. Tartarin, O. Lazar, A. Rumeau, B. Franc, L. Bary, and B. Lambert, "Analysis of drain current transient stability of AlGaN/GaN HEMT stressed under HTOL & HTRB, by random telegraph noise and low frequency noise characterizations," *Microelectron. Reliab.*, vol. 114, Nov. 2020, Art. no. 113895.
- [14] Y. Gu, Y. Wang, J. Chen, B. Chen, M. Wang, and X. Zou, "Temperature-dependent dynamic degradation of carbon-doped GaN HEMTs," *IEEE Trans. Electron Devices*, vol. 68, no. 7, pp. 3290-3295, Jul. 2021.
- [15] Y. C. Chou, D. Leung, I. Smorchkova, M. Wojtowicz, R. Grundbacher, L. Callejo, Q. Kan, R. Lai, P. H. Liu, D. Eng, A. Oki, "Degradation of AlGaN/GaN HEMTs under elevated temperature lifetesting," *Microelectron. Reliab.*, vol. 44, no. 7, pp. 1033-1038, Jul. 2004.
- [16] J. Joh and J. A. D. Alamo, "Critical voltage for electrical degradation of GaN high-electron mobility transistors," *IEEE Electron Device Lett.*, vol. 29, no. 4, pp. 287-289, Apr. 2008.
- [17] C.-Y. Chang, *et al.*, "Electric-field-driven degradation in off-state step-stressed AlGaN/GaN high-electron mobility transistors," *IEEE Trans. Device Mater. Reliab.*, vol. 11, no. 1 pp. 187-193, Mar. 2011.
- [18] E. A. Douglas, *et al.*, "Investigation of the effect of temperature during off-state degradation of AlGaN/GaN high electron mobility transistors," *Microelectron. Reliab.*, vol. 52, no. 1, pp. 23-28, Jan. 2012.
- [19] H. Sun, M. M. Bajo, M. J. Uren, and M. Kuball, "Implications of gate-edge electric field in AlGaN/GaN high electron mobility transistors during off-state degradation," *Microelectron. Reliab.*, vol. 54, no. 12 pp. 2650-2655, Dec. 2014.
- [20] S. DasGupta, M. Sun, A. Armstrong, R. J. Kaplar, M. J. Marinella, J. B. Stanley, S. Atcity, and T. Palacios, "Slow detrapping transients due to gate and drain bias stress in high breakdown voltage AlGaN/GaN HEMTs," *IEEE Trans. Electron Devices*, vol. 59, no. 8, pp. 2115-2122, Aug. 2012.

> REPLACE THIS LINE WITH YOUR MANUSCRIPT ID NUMBER (DOUBLE-CLICK HERE TO EDIT) <

- [21] S. Petitdidier, F. Berthet, Y. Guhel, J.-L. Trolet, P. Mary, C. Gaquière, and B. Boudart, "Characterization and analysis of electrical trap related effects on the reliability of AlInN/GaN HEMTs," *Microelectron. Reliab.*, vol. 55, nos. 9-10, pp. 1719-1723, Aug. 2015.
- [22] M. Rzin, *et al.*, "On-wafer RF stress and trapping kinetics of Fe-doped AlGaIn/GaN HEMTs," *Microelectron. Reliab.*, vols. 88-89, pp. 397-401, Sep. 2018.
- [23] A. Chini, V. D. Lecce, F. Fantini, G. Meneghesso, and E. Zanoni, "Analysis of GaN HEMT failure mechanisms during DC and large-signal RF operation," *IEEE Trans. Electron Devices*, vol. 59, no. 5, pp. 1385-1392, May 2012.
- [24] N. Moulitif, O. Latry, E. Joubert, M. Ndiaye, C. Moreau, J.-F. Goupy, and P. Carton, "Reliability assessment of AlGaIn/GaN HEMTs on the SiC substrate under the RF stress," *IEEE Trans. Power Electron.*, vol. 36, no. 7, pp. 7442-7450, Jul. 2021.
- [25] M. J. Wang, B. Shen, F. J. Xu, Y. Wang, J. Xu, S. Huang, Z. J. Yang, K. Xu, and G. Y. Zhang, "High temperature dependence of the density of two-dimensional electron gas in Al<sub>0.18</sub>Ga<sub>0.82</sub>N/GaN heterostructures," *Appl. Phys. A*, vol. 88, no. 4, pp. 715-718, Jun. 2007.
- [26] A. F. M. Anwar, W. Shangli, and R. T. Webster, "Temperature dependent transport properties in GaN, Al<sub>x</sub>Ga<sub>1-x</sub>N, and In<sub>x</sub>Ga<sub>1-x</sub>N semiconductors," *IEEE Trans. Electron Devices*, vol. 48, no. 3, pp. 567-572, Mar. 2001.
- [27] Y. Q. Tao, D. J. Chen, Y. C. Kong, B. Shen, Z. L. Xie, P. Han, R. Zhang, and Y. D. Zheng, "High-temperature transport properties of 2DEG in AlGaIn/GaN heterostructures," *J. Electron. Mater.*, vol. 35, no. 4, pp. 722-725, Apr. 2006.
- [28] M. Zhao, X. Wang, X. Liu, J. Huang, Y. Zheng, and K. Wei, "Thermal storage of AlGaIn/GaN high-electron-mobility transistors," *IEEE Trans. Device Mater. Reliab.*, vol. 10, no. 3, pp. 360-365, Sep. 2010.
- [29] P. V. Raja, *et al.*, "Comprehensive characterization of vertical GaN-on-GaN Schottky barrier diodes," *Microelectronics J.*, vol. 128, Oct. 2022, Art. no. 105575.
- [30] S. M. Sze and K. K. Ng, "Metal-semiconductor contacts," in *Physics of Semiconductor Devices*, 3rd ed., New Jersey: John Wiley & Sons, 2007, pp. 134-196.
- [31] G. Greco, F. Giannazzo, and F. Roccaforte, "Temperature dependent forward current-voltage characteristics of Ni/Au Schottky contacts on AlGaIn/GaN heterostructures described by a two diodes model," *J. Appl. Phys.*, vol. 121, no. 4, Art. no. 045701, Jan. 2017.
- [32] P. V. Raja and N. V. L. N. Murty, "Thermal annealing studies in epitaxial 4H-SiC Schottky barrier diodes over wide temperature range," *Microelectron. Reliab.*, vol. 87, pp. 213-221, Aug. 2018.
- [33] F. Roccaforte, F. Giannazzo, A. Alberti, M. Spera, M. Cannas, I. Cora, B. Pécz, F. Iucolano, and G. Greco, "Barrier inhomogeneity in vertical Schottky diodes on free standing gallium nitride," *Mater. Sci. Semicond. Process.*, vol. 94, pp. 164-170, May 2019.
- [34] Y. Li, G. I. Ng, S. Arulkumar, G. Ye, Z. H. Liu, K. Ranjan, and K. S. Ang, "Investigation of gate leakage current mechanism in AlGaIn/GaN high-electron-mobility transistors with sputtered TiN," *J. Appl. Phys.*, vol. 121, no. 4, Jan. 2017, Art. no. 044504.
- [35] L. Sang, *et al.*, "Initial leakage current paths in the vertical-type GaN-on-GaN Schottky barrier diodes," *Appl. Phys. Lett.*, vol. 111, no. 12, Sep. 2017, Art. no. 122102.
- [36] S. Turuvekere, N. Karumuri, A. A. Rahman, A. Bhattacharya, A. DasGupta, and N. DasGupta, "Gate leakage mechanisms in AlGaIn/GaN and AlInN/GaN HEMTs: comparison and modeling," *IEEE Trans. Electron Devices*, vol. 60, no. 10, pp. 3157-3165, Oct. 2013.
- [37] D. Yan, H. Lu, D. Cao, D. Chen, R. Zhang, and Y. Zheng, "On the reverse gate leakage current of AlGaIn/GaN high electron mobility transistors," *Appl. Phys. Lett.*, vol. 97, no. 15, Oct. 2010, Art. no. 153503.
- [38] S. Ghosh, A. Dasgupta, A. K. Dutta, Y. S. Chauhan, and S. Khandelwal, "Physics based modeling of gate current including fowler-nordheim tunneling in GaN HEMT," In *IEEE 3rd Int. Conf. Emerg. Electron. (ICEE)*, Dec. 2016.
- [39] D. J. Cheney, *et al.*, "Reliability studies of AlGaIn/GaN high electron mobility transistors," *Semicond. Sci. Technol.*, vol. 28, no. 7, Jun. 2013, Art. no. 074019.
- [40] F. Danesin, A. Tazzoli, F. Zanon, G. Meneghesso, E. Zanoni, A. Cetrionio, C. Lanzieri, S. Lavanga, M. Peroni, and P. Romanini, "Thermal storage effects on AlGaIn/GaN HEMT," *Microelectron. Reliab.*, vol. 48, no. 8-9, pp. 1361-1365, Aug. 2008.
- [41] D. Bisi, M. Meneghini, C. D. Santi, A. Chini, M. Dammann, P. Brueckner, M. Mikulla, G. Meneghesso, and E. Zanoni, "Deep-level characterization in GaN HEMTs-Part I: Advantages and limitations of drain current transient measurements," *IEEE Trans. Electron Devices*, vol. 60, no. 10, pp. 3166-3175, Oct. 2015.
- [42] P. V. Raja, E. Dupouy, M. Bouslama, R. Sommet, J.-C. Nallatamby, "Estimation of trapping induced dynamic reduction in 2DEG density of GaN-based HEMTs by gate-lag DCT technique," *IEEE Trans. Electron Devices*, vol. 69, no. 9, pp. 4864-4869, Jul. 2022.
- [43] G. A. U-Membreno, G. Parish, N. Fichtenbaum, S. Keller, U. K. Mishra, and B. D. Nener, "Electrically active defects in GaN layers grown with and without Fe-doped buffers by metal-organic chemical vapor deposition," *J. Electron. Mater.*, vol. 37, no. 5, pp. 569-572, May 2008.
- [44] M. Silvestri, M. J. Uren, and M. Kuball, "Dynamic transconductance dispersion characterization of channel hot-carrier stressed 0.25- $\mu$ m AlGaIn/GaN HEMTs," *IEEE Trans. Electron Devices*, vol. 33, no. 11, pp. 1550-1552, Nov. 2012.
- [45] M. Silvestri, M. J. Uren, and M. Kuball, "Iron-induced deep-level acceptor center in GaN/AlGaIn high electron mobility transistors: Energy level and cross section," *Appl. Phys. Lett.*, vol. 102, no. 7, Feb. 2013, Art. no. 073501.
- [46] Z.-Q. Fang, D. C. Look, D. H. Kim, and I. Adesida, "Traps in AlGaIn/GaN/SiC heterostructures studied by deep level transient spectroscopy," *Appl. Phys. Lett.*, vol. 87, no. 18, Oct. 2005, Art. no. 182115.
- [47] N. K. Subramani, J. Couvidat, A. A. Hajjar, J.-C. Nallatamby, R. Sommet, and R. Quere, "Identification of GaN buffer traps in microwave power AlGaIn/GaN HEMTs through low frequency S-parameters measurements and TCAD-based physical device simulations," *IEEE J. Electron. Devices Soc.*, vol. 5, no. 3, pp. 175-181, May 2017.



**P. Vigneshwara Raja** received Ph.D. degree from IIT Bhubaneswar, India in 2019. He had postdoc experience (about four years) with XLIM Laboratory France, Ampere Laboratory France, IIT Madras India, Tel Aviv University Israel and University of Aveiro Portugal. Currently, he is an Assistant Professor with the

Department of Electrical Engineering, IIT Dharwad, India. He has published more than 28 research papers in international journals and publications. His current research interests are GaN-based HEMTs, SiC power diodes and MOSFETs, semiconductor radiation detectors, and trap characterization by deep level transient spectroscopy.



**Jean-Christophe NALLATAMBY** is currently Professor at the University of Limoges. His main intensive research is presently focused on the characterization and modeling of semiconductor devices with a special emphasis on TCAD physics-based simulation. He has authored (or) coauthored more than 120

publications in journals and national/international conferences. He serves as a reviewer for several journals. He is a EuMic TPC chair for EuMW 2019 in Paris. He is a general co-chair for the INMMIC organization in 2018 at Brive, France.

> REPLACE THIS LINE WITH YOUR MANUSCRIPT ID NUMBER (DOUBLE-CLICK HERE TO EDIT) <



**Mohamed Bouslama** received the M.Sc. and Ph.D degrees in RF electronic engineering from the University of Limoges, Limoges, France, in 2017 and 2020, respectively. During the Ph.D, his research focuses on low frequency noise characterization, characterization of charge-trapping effects in GaN HEMTs, and understanding its physical behavior using TCAD based device simulation. Currently, his research focuses on the modeling of GaN power devices, and the design of MMIC power amplifier at Thales Research and Technology GIE III-V lab.



**Jean-Claude Jacquet** received the Engineering degree from Institut d'Optique Graduate School - Université Paris-Saclay, France, in 1990. He subsequently joined the Central Research Laboratory of Thales as a Research Staff Member, where he was involved in spintronic devices. He focused his efforts on the giant magnetoresistive effect and found a new physical effect called the magnetorefractive effect. Since 1999, he has been involved in the development of GaInP-HBT and GaN-HEMT microwave power devices at III-V Lab, Palaiseau and is in charge of the thermal and physical modelling using TCAD based device simulation.



**Raphael Sommet** received Ph.D. degree from University of Limoges, France in 1996. Currently, he is a permanent researcher for the CNRS (French National Research Center) at XLIM labs (University of Limoges). Since 2020, he is the head of the team “Nonlinear Microwave Components Circuits and Subsystems”. His research interest concerns GaN HEMT modeling and measurements, 3D thermal modeling and measurements, but also Model Order Reduction, microwave circuit simulation, behavioral modeling and generally the coupling of all physics-based models.



**Benoit Lambert** received the Ph.D. degree from the University of Bordeaux1, Bordeaux, France, in 2001. He joined the European Space Agency, ESTEC center Netherland, as a Component Engineer in charge of millimeter and sub-millimeter wave devices, SiC technologies for power applications, and laser diode. In 2007, he joined United Monolithic Semiconductors Villebon-sur-Yvette, France, as Reliability Engineer in charge of the qualification and space evaluation of new technologies. In 2016, he became reliability expertise manager. Since 2021, he is R&D coordinator for semiconductor and packaging technologies development.